



HAL
open science

Slip rate determined from cosmogenic nuclides on normal-fault facets

Jim Tesson, Lucilla Benedetti, Vincent Godard, Catherine Novaes, Jules Fleury

► **To cite this version:**

Jim Tesson, Lucilla Benedetti, Vincent Godard, Catherine Novaes, Jules Fleury. Slip rate determined from cosmogenic nuclides on normal-fault facets. *Geology*, 2021, 49 (1), pp.66-70. 10.1130/G47644.1 . hal-03453637

HAL Id: hal-03453637

<https://hal.science/hal-03453637v1>

Submitted on 28 Nov 2021

HAL is a multi-disciplinary open access archive for the deposit and dissemination of scientific research documents, whether they are published or not. The documents may come from teaching and research institutions in France or abroad, or from public or private research centers.

L'archive ouverte pluridisciplinaire **HAL**, est destinée au dépôt et à la diffusion de documents scientifiques de niveau recherche, publiés ou non, émanant des établissements d'enseignement et de recherche français ou étrangers, des laboratoires publics ou privés.

Slip rate determined from cosmogenic nuclides on normal-fault facets.

Tracking no: G47644R

Authors:

Jim Tesson (CNRS), Lucilla Benedetti (CNRS), Vincent Godard (Aix-Marseille University), Catherine Novaes (CNRS), Jules Fleury (CNRS), and Team Aster (CNRS)

Abstract:

Facets are major topographic features built over several 100 kyrs above active normal faults. Their development integrates cumulative displacements over a longer timeframe than many other geomorphological markers and they are widespread in diverse extensional settings. We have determined the ^{36}Cl cosmogenic nuclide concentration on limestone faceted spurs at 4 sites in the Central Apennines, representing variable facet height (100-400 m). The ^{36}Cl concentration profiles show nearly constant values over the height of the facet suggesting the facet slope has reached a steady-state equilibrium for ^{36}Cl production. We model the ^{36}Cl build-up on a facet based on a gradual exposure of the sample resulting from fault slip and denudation. Data inversion with this forward model yields accurate constraints on fault slip-rates over the last 20-200 ka, which are in agreement with long-term rate independently determined on some of those faults over the last 1 Ma. ^{36}Cl measurements on faceted spurs can therefore constrain fault slip-rate over time spans that reach up to 200 ka, a time period presently under-sampled in most morpho-tectonic studies.

1 Slip rate determined from cosmogenic nuclides on normal-
2 fault facets.

3 **Jim Tesson¹, Lucilla Benedetti¹, Vincent Godard¹, Catherine Novaes¹, Jules Fleury¹ and**
4 **ASTER Team^{1,1}**

5 *I-Aix Marseille Univ, CNRS, IRD, INRAE, Coll France, CEREGE, Aix-en-Provence, France*

6 **ABSTRACT**

7 Facets are major topographic features built over several 100 kyrs above active normal faults.
8 Their development integrates cumulative displacements over a longer timeframe than many
9 other geomorphological markers and they are widespread in diverse extensional settings. We
10 have determined the ³⁶Cl cosmogenic nuclide concentration on limestone faceted spurs at 4
11 sites in the Central Apennines, representing variable facet height (100-400 m). The ³⁶Cl
12 concentration profiles show nearly constant values over the height of the facet suggesting the
13 facet slope has reached a steady-state equilibrium for ³⁶Cl production. We model the ³⁶Cl
14 build-up on a facet based on a gradual exposure of the sample resulting from fault slip and
15 denudation. Data inversion with this forward model yields accurate constraints on fault slip-
16 rates over the last 20-200 ka, which are in agreement with long-term rate independently
17 determined on some of those faults over the last 1 Ma. ³⁶Cl measurements on faceted spurs
18 can therefore constrain fault slip-rate over time spans that reach up to 200 ka, a time period
19 presently under-sampled in most morpho-tectonic studies.

20 **INTRODUCTION**

21 Facets are characteristic landforms associated with the activity of normal faults (Wallace
22 1978, Armijo et al. 1986). But their potential as tectonic markers and the possibility of
23 retrieving quantitative information on long-term slip rates from their morphological attributes
24 and rates of evolution have seldom been considered (Petit et al. 2009, Tucker et al.
25 2011). This is an attractive prospect, as faceted spur development integrates cumulative
26 displacements over a longer timeframe (100's of ka) than most other geomorphological
27 markers and are ubiquitous in uplifting landscapes bounded by active normal faults.
28 Quantifying tectonic deformation over Quaternary timescales usually relies on the analysis of
29 passive morphological markers formed by various types of processes, such as fluvial or

¹*G. Aumaître, D.L. Bourlès, K. Keddadouche*

30 marine terraces, moraines and landslides. In many settings the temporal record of such
31 markers spans only a few 10 ka, leaving the 100 ka timescale usually poorly documented
32 (Ryerson et al. 2006, Gold et al. 2016), which is a major hindrance for our understanding of
33 how deformation is accommodated. Triangular facets, on the other hand, are not passively
34 deformed markers but result from the combination of sustained rock uplift of the normal fault
35 footwall and its long-term erosion (Burbank and Anderson 2011).

36 Here, we provide the first systematic investigation of the use of the ^{36}Cl cosmogenic
37 nuclide to assess the rates of facet evolution. Our goal is to link cosmogenic nuclide buildup
38 on limestone faceted spurs and fault slip-rate by investigating 4 sites in the Central
39 Apennines, Italy of different shape and height (Fig 1). Following on Tucker et al. (2011)'s
40 assumptions linking facet slope, denudation rate and fault slip-rate, we compute the
41 theoretical ^{36}Cl concentration buildup of a facet as a function of its evolution with time (Fig.
42 2). The inversion of data acquired from the 4 studied sites demonstrates that our approach
43 provides accurate constraints on fault slip rates over time-spans ≤ 200 ka (Fig. 3 and 4).

44 **1- THEORETICAL ^{36}Cl BUILD UP ON A TRIANGULAR FACET**

45

46 Faceted spurs are near planar triangular or trapezoidal surfaces produced by the erosion of
47 normal fault scarps that are continuously rejuvenated at their base by sustained slip (Wallace
48 1978). Here we focus on normal fault footwalls formed in resistant bedrock and undergoing a
49 weathering-limited evolution (Tucker et al. 2011). Morphological evolution models (Tucker
50 et al. 2011, Strak et al. 2011, Tucker et al. 2020) suggest facet morphology reflects an
51 equilibrium between rock uplift from fault slip and erosion.

52 At the base of the facets, well-preserved bedrock fault scarps representing the cumulative
53 displacement on the fault since the last glacial maximum can be observed (Wallace 1978,
54 Armijo et al. 1992). This has been confirmed in the Mediterranean by exposure-age dating in
55 Greece, Italy, Israel, Turkey (e.g. Benedetti et al. 2013, Cowie et al. 2017). Post-glacial
56 changes in climatic conditions result in a decrease in hillslope erosion rates and preservation
57 of those bedrock fault scarps (Armijo et al. 1998, Allen et al. 1999). The timing of this shift is
58 not accurately dated and may spatially vary. In the Apennines, it is estimated to be 12-21 ka
59 (Giraudi 2017).

60 Based on these previous observations we use a two-stage kinematic model to predict ^{36}Cl
61 buildup in material currently exposed along the facet surface. First, under glacial conditions,
62 we assume topographic steady state, such that rock uplift of the footwall is equal to the

63 denudation rate of the facet surface. Rock sample are progressively exhumed parallel to the
64 slip vector at a rate set by the fault slip-rate (Fig 2). Second, in post glacial conditions, we
65 assume denudation of the facet to be negligible, such that rock samples are continuously
66 exposed at the surface, with no significant regolith cover (Tucker et al., 2011).

67 Our approach relies on the interpretation of measured ^{36}Cl concentration at the surface in
68 terms of this exhumation and exposure history of the facet. Based on the conceptual evolution
69 described above, we parametrize this evolution using the time at which the sample starts
70 moving towards the surface (T_{exhum}), the rate at which the sample moves parallel to fault
71 motion prior to post-glacial conditions (SR), and the duration of post-glacial exposure
72 assumed without erosion (T_{pg}). We combine this simple model with equations describing
73 cosmogenic nuclides buildup to predict ^{36}Cl concentrations at the surface of the facet for any
74 combination of the 3 parameters (T_{exhum} , T_{pg} , SR) defining the prescribed history (Suppl.).

75 2- ^{36}Cl CONCENTRATION PROFILES ON 4 FACETED SPURS IN CENTRAL 76 APENNINES

77 We focus on 4 facets formed in limestones located along 3 active faults in central Apennines
78 (Italy). Since late Pliocene-early Pleistocene, active normal faults accommodate the SW-NE
79 extension in the area (Roberts and Michetti 2004). The Velino-Magnola fault is a major
80 structure of the range (~30 km long, Fig. 1) with facets up to 300-800 m high, where we
81 sampled two sites MA1 and MA3 along the northern and central part of the fault,
82 respectively. The Roccapreturo fault is shorter (10 km), with lower facets (100-150 m), and
83 was sampled at site AR in the center of the fault. The Bazzano fault is a small (3 km long)
84 antithetic fault, with several facets reaching 100-150 m high, sampled in its southern section
85 at site BAZ (Suppl.). The surface of the 4 sampled facets displays regular slope $30\text{-}35^\circ$ (Fig
86 3). The surface of the facet is characterized by an alternance of bedrock outcrop, small
87 bedrock protrusions (< 1m high), and patches of soil and screes less than a few cm thick. The
88 facets are generally bounded by entrenched non-perennial streams that flow perpendicular to
89 the fault's strike, which suggests recent incision that is contemporaneous with fault
90 development. The slopes of the colluvial wedge surface ($\alpha\sim 25\text{-}30$) and of the facets ($\gamma\sim 30\text{-}35$)
91 are similar across sites, the fault dips (β) from 40° at MA1, to 65° at BAZ (Suppl.).

92 The facets were sampled following an up-dip fault transect (Suppl.). We focused sampling on
93 the lower part of the facet, where the surface appears less rugged, and near the facet center to
94 avoid increased erosion by bounding gullies. Samples are 5-10 cm thick pieces of bedrock,
95 taken on the top of protruding (> 0.5 m) bedrock surfaces, avoiding places that could have

96 been covered by regolith. Each sample was chemically prepared for ^{36}Cl measurements
97 (Suppl.). At MA3 and ARC, the ^{36}Cl concentrations are roughly constant all along the facet
98 (Fig. 3), except at the base where they increase by about 30%. At MA1 and BAZ, facets are
99 lower and there are fewer points of measurements, but we observe a similar pattern at MA1
100 with constant values at the top, a slight decrease and an abrupt increase at the base of facet.
101 There are only 3 data points at BAZ with decreasing concentrations toward the base. The
102 ^{36}Cl concentrations along all studied facets are thus roughly constant suggesting that the
103 denudation rate on those features is approximately constant. This observation is consistent
104 with a facet development model that assumes a constant denudation rate. Moreover while it
105 has been usually assumed that erosion would vary with facet height (Tucker et al. 2020 and
106 references there in), our results suggest that, on the facet we studied, this is not the case.

107 **3-FAULT SLIP-RATE FROM ^{36}Cl DATA INVERSION**

108 To constrain the fault slip-rate we carried out a Bayesian inversion of the observed ^{36}Cl
109 concentrations where the model parameters are the individual slip-rates of the faults (SR_{MA3} ,
110 SR_{MA1} , SR_{ARC} , SR_{BAZ}), and the post-glacial period duration (T_{PG}), assumed to be the same for
111 the 4 sites (T_{exhum} is fixed a priori see suppl.). A complete description of the inversion
112 procedure using the GW-MCMC algorithm (Goodman and Weare 2010), the corresponding
113 parameters and the numerical code are provided in the Suppl. The inversion yielded mean
114 slip-rates of 3.0 ± 1.2 mm/yr for MA3, 0.2 ± 0.02 mm/yr for MA1, 0.4 ± 0.3 mm/yr for ARC,
115 and 0.06 ± 0.02 mm/yr for BAZ (Fig. 3 and 4). The mean post-glacial duration, common to all
116 sites, is 18.7 ± 2 ka.

117 The modeled ^{36}Cl concentrations recover the average observed values at the scale of the facet,
118 but do not account for the variability in ^{36}Cl concentrations observed in the lower part of the
119 transects (Fig. 3).

120 **4-DISCUSSION**

121 **Local controls on ^{36}Cl concentration**

122 In most cases, for the upper part, the inversion reproduces the mean ^{36}Cl concentration.
123 Overall, the discrepancy between observed and modeled concentrations is at most 0.5×10^5 at
124 $^{36}\text{Cl}/\text{g}$ rock except for the points at the base of each site where observed concentrations are
125 systematically higher by as much as 20% (except BAZ). The discrepancy for the upper part of
126 the profile could be attributed to the stochastic dynamics of local processes such as temporary
127 cover by a few cm of scree or abrupt removal of bedrock fragments that would lower the
128 observed amount of ^{36}Cl with respect to the predictions of our model. A scree cover of 10 cm

129 would yield a 10% decrease in ^{36}Cl concentration and could account for a large fraction of the
130 observed intra-site variability (Suppl.). On the contrary, simulations for MA3 show that a
131 scree cover of less than 5-10 cm yields an increase in [^{36}Cl]. This is due to a relatively large
132 slip-rate (3 mm/yr), and high natural chlorine content of some samples (>50 ppm) that
133 maximize ^{36}Cl production at depth 0 to 100 cm (Schimmelpfennig et al. 2009). Another
134 possibility that explains such a discrepancy could be that the facet slope might be locally
135 steeper than the mean value used in the model. A difference of 10° could increase ^{36}Cl
136 concentration by about 7% (Suppl.). At the base of the profile, where observed concentrations
137 are systematically higher by as much as 20% (except BAZ), the observed systematic increase
138 in ^{36}Cl concentration cannot be attributed to such short wavelength random variability in
139 surface processes. This portion is at the intersection between the bedrock scarp and the facet
140 slope, which is defined in the model by the altitude of the bedrock scarp top. There is a high
141 uncertainty in the altitude of this point, usually affected by sliding scree that could explain the
142 discrepancy. The shielding calculation might also underestimate the effect of secondary
143 neutrons produced through colluvial material or bedrock (Masarik and Wieler 2003, Balco
144 2014). The colluvial density and the dip of the colluvial slope also affect the ^{36}Cl content at
145 the base of the profile and could additionally account for this discrepancy (Suppl.).

146 **Duration of exhumation versus post-glacial exposure**

147 The value of 18.7 ± 2 ka obtained for the post-glacial duration is consistent with the timing of
148 the most important glacial retreat in the Apennines estimated at about 21 ka from lake
149 deposits records and morainic deposit (Giraudi 2017). It also corroborates the exposure ages
150 from the top of the bedrock scarp at 11-15 ka at similar sites around the Apennines (Benedetti
151 et al. 2013, Cowie et al. 2017). The amount of ^{36}Cl accumulated during the exhumation phase
152 under glacial conditions is controlled primarily by fault slip rates and accounts for 9% of the
153 total ^{36}Cl budget for MA3, 58% for MA1, 24% for ARC and 66% for BAZ. It means that at
154 MA3, 95% of the measured ^{36}Cl has been accumulated over the last 20 ka, at the other sites
155 this integration time is much longer, with durations of 185 ka, 47 ka and 210 ka at MA1, ARC
156 and BAZ, respectively. Our approach thus allows determining slip-rates averaged over time
157 scales that range from 20 to 210 ka. It is noteworthy that slower slip-rates are more tightly
158 constrained because the ^{36}Cl buildup at depth outweigh the post-glacial ^{36}Cl production.

159 **Slip-rate variability over time and relationships with facet morphology**

160 Slip-rates derived from inversion for the four studied sites are between 3 and 0.06 mm/yr
161 which is within the range of observations over the Holocene for similar faults in the
162 Apennines (Benedetti et al. 2013, Cowie et al. 2017). Sites MA3 and MA1 are less than 5 km

163 apart and located on two segments of the Magnola fault (Suppl.). ^{36}Cl exposure dating of the
164 bedrock scarp at each site yield Holocene-averaged slip rates of 1 to 1.5 mm/yr at MA3 and
165 MA1 (Schlagenhauf et al. 2011), which is comparable with the result obtained at MA3 (3 ± 1.2
166 mm/yr over 20 ka). On the other hand, the slip-rate at MA1 (0.2 ± 0.02 mm/yr over 185 ka) is
167 much lower than the one determined over the last ≈ 15 ka by Schlagenhauf et al. (2011). This
168 discrepancy may be related to the difference in time-scale, suggesting that the slip on the fault
169 has considerably accelerated over the last ≈ 15 ka. Slip-rate variability through time has
170 already been reported for the few faults worldwide where multiple time-scales records are
171 available (Perouse and Wernicke 2017, Friedrich et al. 2003). Studies on normal fault growth
172 have shown that slip-rate can be highly variable over the fault length and over time
173 (Manighetti et al. 2005). Our results confirm those observations and provide data to link
174 incremental earthquake slip events and fault growth. The Bazzano fault (site BAZ) is an
175 antithetic fault of the Paganica fault that ruptured during the 2009 L'Aquila earthquake.
176 Several studies have allowed determining the Paganica slip-rate over a few thousand years to
177 the Middle Pleistocene (Pucci et al. 2019). All converge toward a slip-rate of less than 0.4
178 mm/yr. The rate obtained for the antithetic Bazzano fault of 0.06 ± 0.02 mm/yr over the last
179 210 ka would thus account for about 15% of the Paganica synthetic fault slip, which appears
180 realistic (Boncio et al. 2010). The slip-rate at site AR of 0.4 ± 0.3 mm/yr over the last 47 ka is
181 similar to the rate previously estimated from Falcucci et al. (2015) of 0.2-0.3 mm/yr over the
182 last 1 ± 0.2 Ma.

183 The slip-rates obtained for the four sites vary with the facet height, with the highest rate at
184 MA3 where facet is 800 m-high (Schlagenhauf et al. 2011). This is in agreement with DePolo
185 and Anderson (2000) who carried out a statistical analysis on normal faults located in the
186 Basin and Range and observed a logarithmic relationship between the height of the facet and
187 the vertical slip-rate of the fault (ranging from 0.001 to 2 mm/yr). Based on numerical
188 modelling experiments, Petit et al. (2009) and Strak et al. (2011) also derived a linear
189 relationship between facet height and throw rate in agreement with our results.

190 **CONCLUSIONS**

191 Our study presents the first systematic CRN measurements across facets developed above
192 normal faults. We observe strikingly consistent signals with near constant ^{36}Cl concentrations
193 over the height of the studied facets, which suggests the facets are close to a morphological
194 steady state with a constant denudation during their development. Accordingly, we performed
195 inverse modeling of the concentration profiles and inferred slip rates over the last 20-200 ka,
196 the results of which are in agreement with long-term rate independently determined on some

197 of those faults over the last 1 Ma. The integration time span for ^{36}Cl accumulation over the
198 facets is longer than the postglacial history of these landscapes, suggesting that such
199 measurements could provide slip rates estimates over a time window that is usually
200 undersampled in most tectonic geomorphology studies.

201 **ACKNOWLEDGMENTS**

202 This work has been partly funded by the LABEX OT MED. M. Rizza and B. Ourion are
203 greatly acknowledged for their help and support in the field.

204 **FIGURES CAPTIONS**

205 Fig. 1 : A) Tectonic map of the Lazio-Abruzzo fault system (Schlagenhauf et al. 2011,
206 Benedetti et al. 2013) with the faults (red line) bounding the sampled facets (yellow arrows)
207 and site names (sites names were kept as in Schlagenhauf et al. 2010). B) Photography of the
208 F-MA1 facet with location of samples and Holocene bedrock fault scarp at the base of the
209 facets.

210 Fig. 2 : A-Modelled topographic profile of normal escarpment following Tucker et. al (2011)
211 model resulting from exhumation of the footwall, with slope of the colluvial wedge surface α ,
212 dipping angle of fault-plane β , and γ slope of facet surface.

213 Fig. 3 : Measured (black dot) and modeled ^{36}Cl concentrations obtained from Bayesian
214 inversion (grey pdf) of samples collected on the 4 facets (MA3, MA1, AR, BAZ) in Central
215 Italy, as a function of sample altitude. Reduced chi-squared values are MA3=6.4; MA1=8.2;
216 AR=5.2; BAZ=19.6.

217 Fig. 4 : Results from Bayesian inversion of ^{36}Cl data acquired on facet. Probability densities
218 are plotted as function of slip-rate and post-glacial period duration (T_{pg}), with contour lines
219 representing 10, 30, 50, 70, 90 % highest density interval. Pdf of posterior distribution is also
220 shown for each SR and for T_{pg} .

221 **REFERENCES CITED**

222 Allen, J. R. M. et al. Rapid environmental changes in southern Europe during the last glacial
223 period. *Nature* 400, 740–743 (1999).

224 Armijo, R., Tapponnier, P., Mercier, J. L., & Han, T. L. (1986). Quaternary extension in
225 southern Tibet: Field observations and tectonic implications. *Journal of Geophysical*
226 *Research: Solid Earth*, 91(B14), 13803-13872.

227

228 Armijo, R., Lyon-Caen, H., & Papanastassiou, D. (1992). East-west extension and Holocene
229 normal-fault scarps in the Hellenic arc. *Geology*, 20(6), 491-494.
230

231 Balco, G. (2014). Simple computer code for estimating cosmic-ray shielding by oddly shaped
232 objects. *Quaternary Geochronology*, 22, 175-182.
233

234 Benedetti, L., Manighetti, I., Gaudemer, Y., Finkel, R., Malavieille, J., Pou, K., ... &
235 Keddadouche, K. (2013). Earthquake synchrony and clustering on Fucino faults (Central
236 Italy) as revealed from in situ ³⁶Cl exposure dating. *Journal of Geophysical Research: Solid
237 Earth*, 118(9), 4948-4974.
238

239 Boncio, P., Pizzi, A., Brozzetti, F., Pomposo, G., Lavecchia, G., Di Naccio, D., & Ferrarini,
240 F. (2010). Coseismic ground deformation of the 6 April 2009 L'Aquila earthquake (central
241 Italy, Mw6. 3). *Geophysical Research Letters*, 37(6).
242

243 Burbank, D. W., & Anderson, R. S. (2011). *Tectonic geomorphology*. John Wiley & Sons.
244

245 Cowie, P. A., Phillips, R. J., Roberts, G. P., McCaffrey, K., Zijerveld, L. J. J., Gregory, L. C.,
246 ... & Freeman, S. P. H. T. (2017). Orogen-scale uplift in the central Italian Apennines drives
247 episodic behaviour of earthquake faults. *Scientific reports*, 7, 44858.
248

249 DePolo, C. M., & Anderson, J. G. (2000). Estimating the slip rates of normal faults in the
250 Great Basin, USA. *Basin Research*, 12(3-4), 227-240.
251

252 Friedrich, A. M., Wernicke, B. P., Niemi, N. A., Bennett, R. A., & Davis, J. L. (2003).
253 Comparison of geodetic and geologic data from the Wasatch region, Utah, and implications
254 for the spectral character of Earth deformation at periods of 10 to 10 million years. *Journal of
255 Geophysical Research: Solid Earth*, 108(B4).
256

257 Giraudi, C., & Giaccio, B. (2017). Middle Pleistocene glaciations in the Apennines, Italy: new
258 chronological data and preservation of the glacial record. *Geological Society, London, Special
259 Publications*, 433(1), 161-178.
260

261 Gold, R. D., Cowgill, E., Arrowsmith, J. R., & Friedrich, A. M. (2017). Pulsed strain release
262 on the Altyn Tagh fault, northwest China. *Earth and Planetary Science Letters*, 459, 291-300.
263

264 Goodman, J., & Weare, J. (2010). Ensemble samplers with affine
265 invariance. *Communications in applied mathematics and computational science*, 5(1), 65-80.
266

267 Mitchell, S. G., Matmon, A., Bierman, P. R., Enzel, Y., Caffee, M., & Rizzo, D. (2001).
268 Displacement history of a limestone normal fault scarp, northern Israel, from cosmogenic
269 ^{36}Cl . *Journal of Geophysical Research: Solid Earth*, 106(B3), 4247-4264.
270

271 Masarik, J., & Wieler, R. (2003). Production rates of cosmogenic nuclides in boulders. *Earth
272 and Planetary Science Letters*, 216(1-2), 201-208.
273

274 Manighetti, I., Campillo, M., Sammis, C., Mai, P. M., & King, G. (2005). Evidence for self-
275 similar, triangular slip distributions on earthquakes: Implications for earthquake and fault
276 mechanics. *Journal of Geophysical Research: Solid Earth*, 110(B5).
277

278 Petit, C., Gunnell, Y., Gonga-Saholiariliva, N., Meyer, B., & Séguinot, J. (2009b). Faceted
279 spurs at normal fault scarps: Insights from numerical modeling. *Journal of Geophysical
280 Research: Solid Earth*, 114(B5).
281

282 Pérouse, E., & Wernicke, B. P. (2017). Spatiotemporal evolution of fault slip rates in
283 deforming continents: The case of the Great Basin region, northern Basin and Range
284 province. *Geosphere*, 13(1), 112-135.
285

286 Pucci, S., Villani, F., Civico, R., Di Naccio, D., Porreca, M., Benedetti, L., ... & Pantosti, D.
287 (2019). Complexity of the 2009 L'Aquila earthquake causative fault system (Abruzzi
288 Apennines, Italy) and effects on the Middle Aterno Quaternary basin
289 arrangement. *Quaternary Science Reviews*, 213, 30-66.
290

291 Roberts, G. P., and A. M. Michetti (2004), Spatial and temporal variations in growth rates
292 along active normal fault systems: an example from The Lazio–Abruzzo Apennines, central
293 Italy, *J. Struct. Geol.*, 26(2), 339–376, doi:10.1016/S0191-8141(03)00103-2.
294

295 Roberts, G. P., Raithatha, B., Sileo, G., Pizzi, A., Pucci, S., Walker, J. F., ... & Guerrieri, L.
296 (2010). Shallow subsurface structure of the 2009 April 6 M w 6.3 L'Aquila earthquake
297 surface rupture at Paganica, investigated with ground-penetrating radar. *Geophysical Journal*
298 *International*, 183(2), 774-790.

299

300 Ryerson, F.J., Tapponnier, P., Finkel, R.C., Mériaux, A.-S., Van der Woerd, J., Lasserre, C.,
301 Chevalier, M.-L., Xu, X., Li, H., and King, G.C.P., 2006, Applications of morphochronology
302 to the active tectonics of Tibet, in Siame, L.L., Bourlès, D.L., and Brown, E.T., eds.,
303 Application of cosmogenic nuclides to the study of Earth surface processes: The practice and
304 the potential: Geological Society of America Special Paper 415, p. 61–86, doi:
305 10.1130/2006.2415(05).

306

307 Schimmelpfennig, I., Benedetti, L., Finkel, R., Pik, R., Blard, P. H., Bourles, D., ... &
308 Williams, A. (2009). Sources of in-situ ³⁶Cl in basaltic rocks. Implications for calibration of
309 production rates. *Quaternary Geochronology*, 4(6), 441-461.

310

311 Schlagenhauf, A., Gaudemer, Y., Benedetti, L., Manighetti, I., Palumbo, L.,
312 Schimmelpfennig, I., ... & Pou, K. (2010). Using in situ Chlorine-36 cosmonuclide to recover
313 past earthquake histories on limestone normal fault scarps: a reappraisal of methodology and
314 interpretations. *Geophysical Journal International*, 182(1), 36-72.

315

316 Schlagenhauf, A., Manighetti, I., Benedetti, L., Gaudemer, Y., Finkel, R., Malavieille, J., &
317 Pou, K. (2011). Earthquake supercycles in Central Italy, inferred from ³⁶Cl exposure
318 dating. *Earth and Planetary Science Letters*, 307(3-4), 487-500.

319

320 Strak, V., Dominguez, S., Petit, C., Meyer, B., & Loget, N. (2011). Interaction between
321 normal fault slip and erosion on relief evolution: Insights from experimental
322 modelling. *Tectonophysics*, 513(1-4), 1-19.

323

324 Tucker, G. E., McCoy, S. W., Whittaker, A. C., Roberts, G. P., Lancaster, S. T., & Phillips, R.
325 (2011). Geomorphic significance of postglacial bedrock scarps on normal-fault
326 footwalls. *Journal of Geophysical Research: Earth Surface*, 116(F1).

327

328 Tucker, G. E., Hobbey, D. E., McCoy, S. W., & Struble, W. T. Modeling the Shape and
329 Evolution of Normal-Fault Facets. *Journal of Geophysical Research: Earth Surface*,
330 e2019JF005305.

331

332 Wallace, R. E. (1978). Geometry and rates of change of fault-generated range fronts, north-
333 central Nevada. *J. Res. US Geol. Surv*, 6(5), 637-650.

334

Figure 1

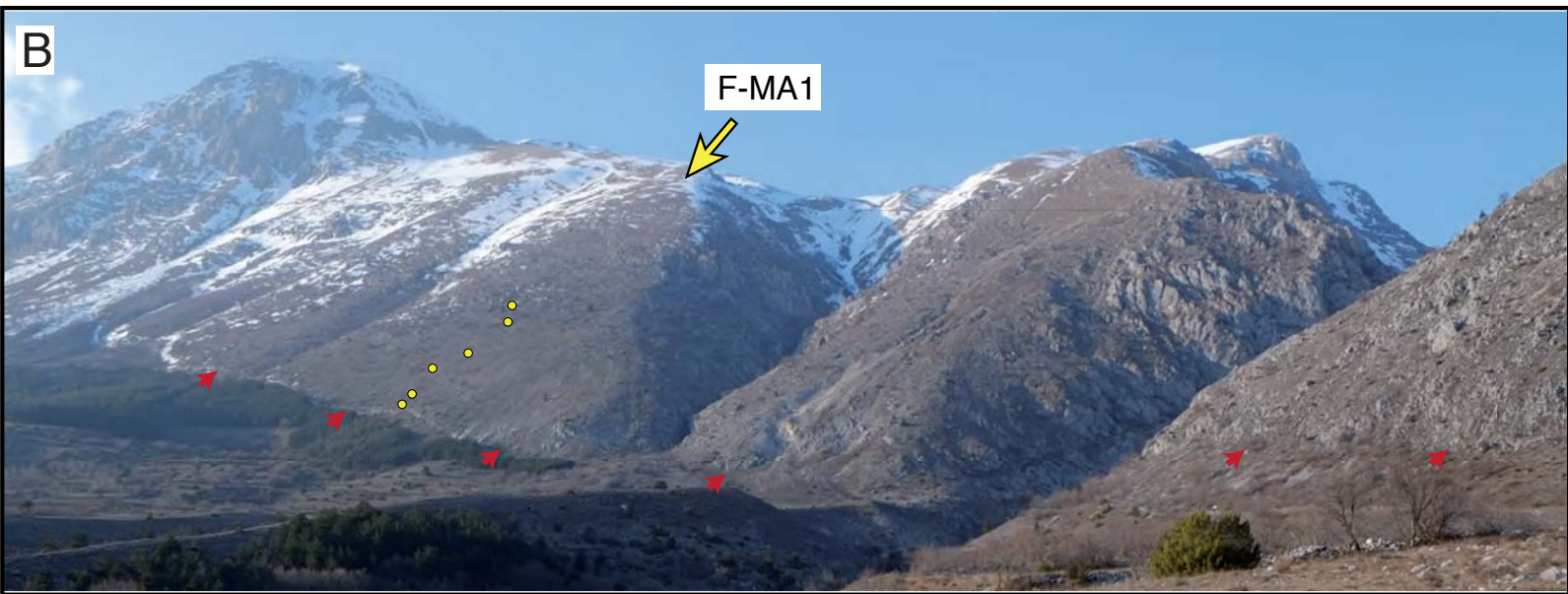
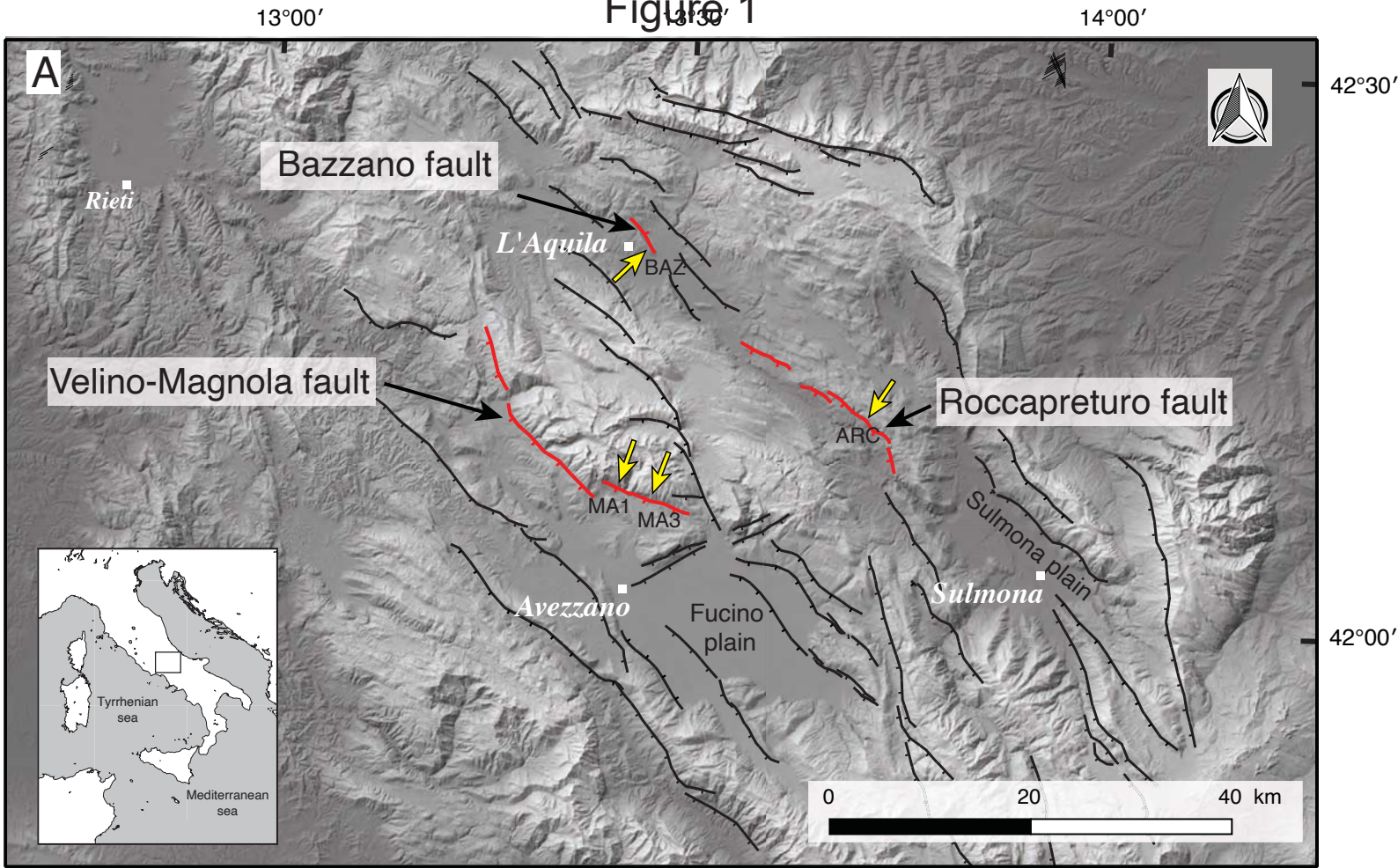


Figure 2

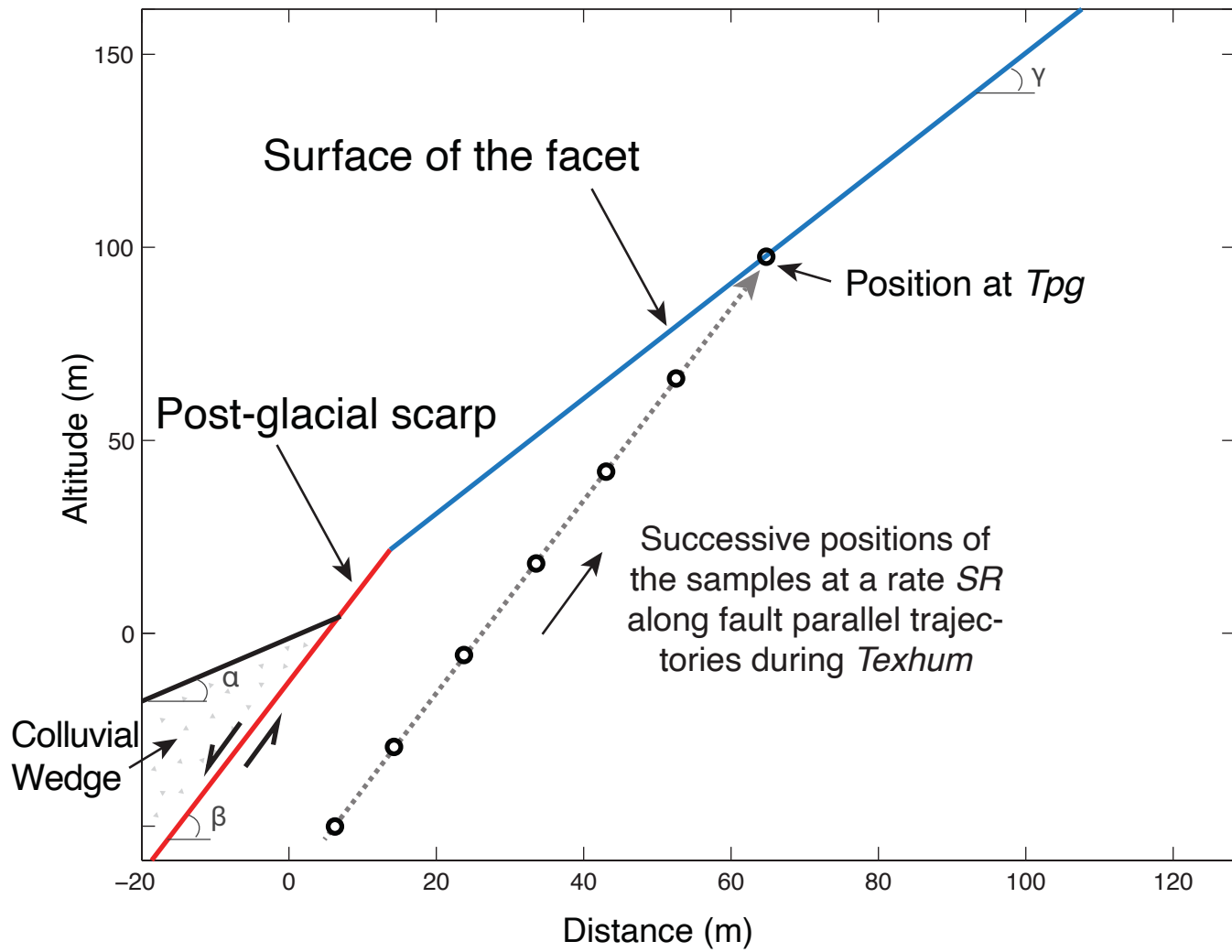


Figure 3

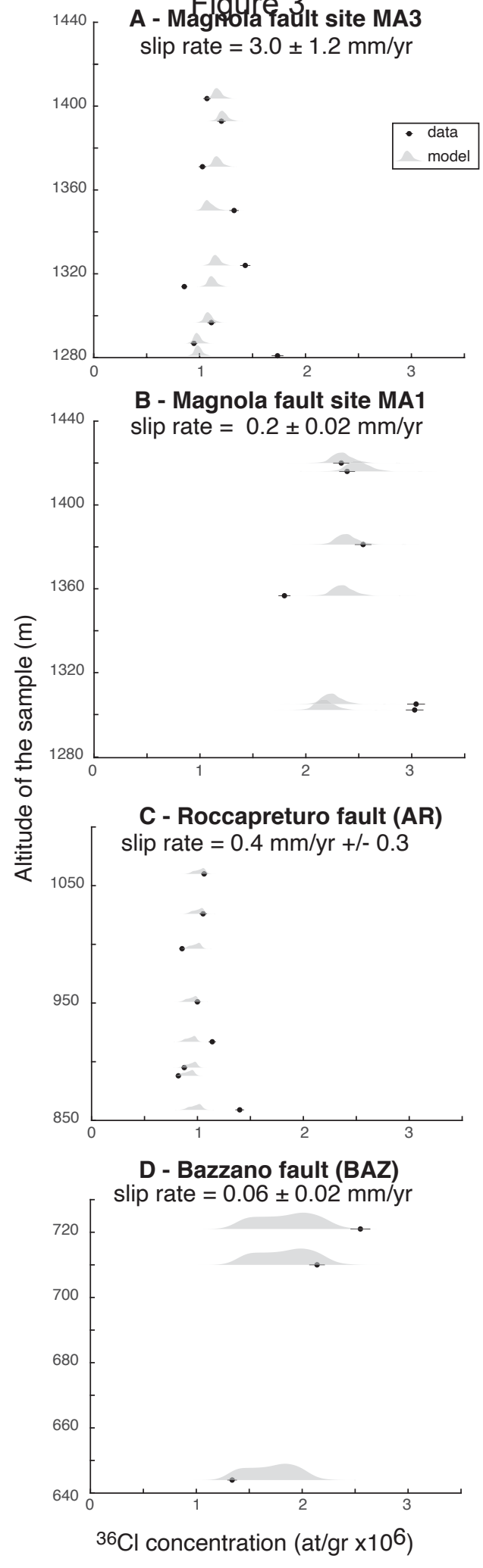
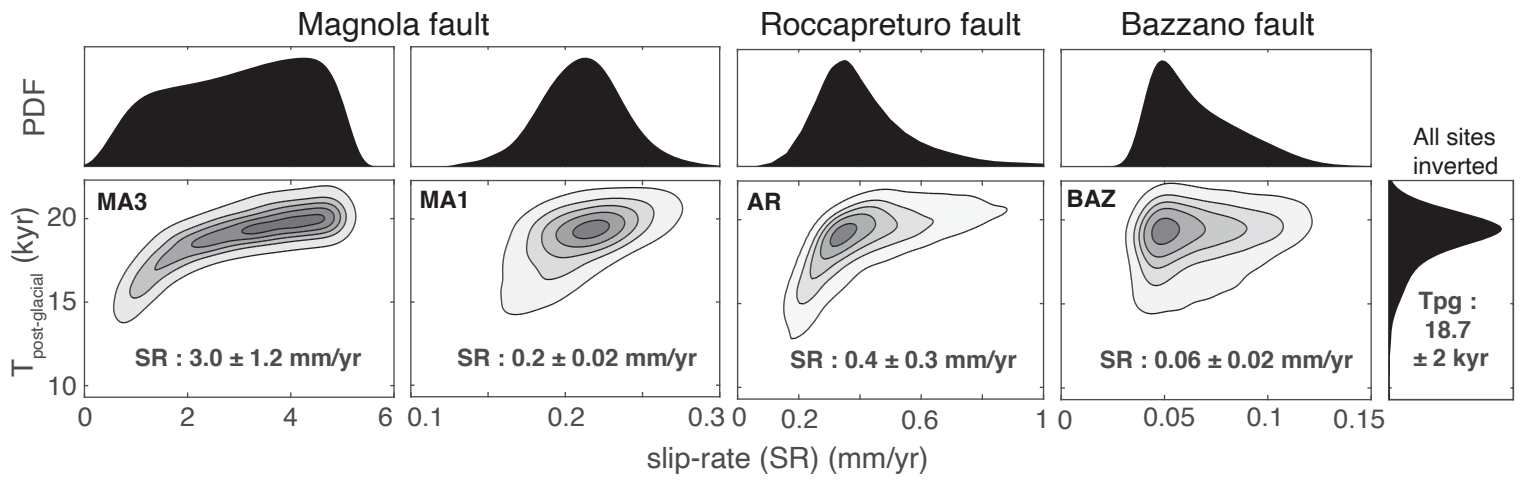


Figure 4



1 Slip rate determined from cosmogenic nuclides on normal-
2 fault facets.

3 **Jim Tesson¹, Lucilla Benedetti¹, Vincent Godard¹, Catherine Novaes¹, Jules Fleury¹ and**
4 **ASTER Team^{1,1}**

5 *I-Aix Marseille Univ, CNRS, IRD, INRAE, Coll France, CEREGE, Aix-en-Provence, France*

6 **ABSTRACT**

7 Facets are major topographic features built over several 100 kyrs above active normal faults.
8 Their development integrates cumulative displacements over a longer timeframe than many
9 other geomorphological markers and they are widespread in diverse extensional settings. We
10 have determined the ³⁶Cl cosmogenic nuclide concentration on limestone faceted spurs at 4
11 sites in the Central Apennines, representing variable facet height (100-400 m). The ³⁶Cl
12 concentration profiles show nearly constant values over the height of the facet suggesting the
13 facet slope has reached a steady-state equilibrium for ³⁶Cl production. We model the ³⁶Cl
14 build-up on a facet based on a gradual exposure of the sample resulting from fault slip and
15 denudation. Data inversion with this forward model yields accurate constraints on fault slip-
16 rates over the last 20-200 ka, **which** are in agreement with long-term rate independently
17 determined on some of those faults over the last 1 Ma. ³⁶Cl measurements on faceted spurs
18 can therefore constrain fault slip-rate over time spans that reach up to 200 ka, a time period
19 presently under-sampled in most morpho-tectonic studies.

20 **INTRODUCTION**

21 Facets are characteristic landforms associated with the activity of normal faults (Wallace
22 1978, Armijo et al. 1986). But their potential as tectonic markers and the possibility of
23 retrieving quantitative information on long-term slip rates from their morphological attributes
24 and rates of evolution have seldom been considered (Petit et al. 2009, Tucker et al.
25 2011). This is an attractive prospect, as faceted spur development integrates cumulative
26 displacements over a longer timeframe (100's of ka) than most other geomorphological
27 markers and are ubiquitous in uplifting landscapes bounded by active normal faults.
28 Quantifying tectonic deformation over Quaternary timescales usually relies on the analysis of
29 passive morphological markers formed by various types of processes, such as fluvial or

¹*G. Aumaître, D.L. Bourlès, K. Keddadouche*

30 marine terraces, moraines and landslides. In many settings the temporal record of such
31 markers spans only a few 10 ka, leaving the 100 ka timescale usually poorly documented
32 (Ryerson et al. 2006, Gold et al. 2016), which is a major hindrance for our understanding of
33 how deformation is accommodated. Triangular facets, on the other hand, are not passively
34 deformed markers but result from the combination of sustained rock uplift of the normal fault
35 footwall and its long-term erosion (Burbank and Anderson 2011).

36 Here, we provide the first systematic investigation of the use of the ^{36}Cl cosmogenic
37 nuclide to assess the rates of facet evolution. Our goal is to link cosmogenic nuclide buildup
38 on limestone faceted spurs and fault slip-rate by investigating 4 sites in the Central
39 Apennines, Italy of different shape and height (Fig 1). Following on Tucker et al. (2011)'s
40 assumptions linking facet slope, denudation rate and fault slip-rate, we compute the
41 theoretical ^{36}Cl concentration buildup of a facet as a function of its evolution with time (Fig.
42 2). The inversion of data acquired from the 4 studied sites demonstrates that our approach
43 provides accurate constraints on fault **slip rates over time-spans ≤ 200 ka** (Fig. 3 and 4).

44 **1- THEORETICAL ^{36}Cl BUILD UP ON A TRIANGULAR FACET**

45

46 Faceted spurs are near planar triangular or trapezoidal surfaces **produced by the erosion of**
47 **normal fault scarps** that are continuously rejuvenated at their base by sustained slip (Wallace
48 1978). Here we focus on normal fault footwalls formed in resistant bedrock and undergoing a
49 weathering-limited evolution (Tucker et al. 2011). Morphological evolution models (Tucker
50 et al. 2011, Strak et al. 2011, Tucker et al. 2020) suggest facet morphology reflects an
51 equilibrium **between rock uplift from fault slip and erosion**.

52 At the base of the facets, well-preserved bedrock fault scarps representing the cumulative
53 displacement on the fault since the last glacial maximum can be observed (Wallace 1978,
54 Armijo et al. 1992). This has been confirmed in the Mediterranean by exposure-age dating in
55 Greece, Italy, Israel, Turkey (e.g. Benedetti et al. 2013, Cowie et al. 2017). **Post-glacial**
56 **changes** in climatic conditions result in a decrease in hillslope erosion rates and preservation
57 of those bedrock fault scarps (Armijo et al. 1998, Allen et al. 1999). The timing of this shift is
58 not accurately dated and **may spatially vary**. In the Apennines, it is estimated to be 12-21 ka
59 (Giraudi 2017).

60 Based on these previous observations we use a two-stage kinematic model to predict ^{36}Cl
61 buildup in material currently exposed along the facet surface. First, under glacial conditions,
62 **we assume topographic steady state, such that rock uplift of the footwall is equal to the**

63 denudation rate of the facet surface. Rock sample are progressively exhumed parallel to the
64 slip vector at a rate set by the fault slip-rate (Fig 2). Second, in post glacial conditions, we
65 assume denudation of the facet to be negligible, such that rock samples are continuously
66 exposed at the surface, with no significant regolith cover (Tucker et al., 2011).

67 Our approach relies on the interpretation of measured ^{36}Cl concentration at the surface in
68 terms of this exhumation and exposure history of the facet. Based on the conceptual evolution
69 described above, we parametrize this evolution using the time at which the sample starts
70 moving towards the surface (T_{exhum}), the rate at which the sample moves parallel to fault
71 motion prior to post-glacial conditions (SR), and the duration of post-glacial exposure
72 assumed without erosion (T_{pg}). We combine this simple model with equations describing
73 cosmogenic nuclides buildup to predict ^{36}Cl concentrations at the surface of the facet for any
74 combination of the 3 parameters (T_{exhum} , T_{pg} , SR) defining the prescribed history (Suppl.).

75 2- ^{36}Cl CONCENTRATION PROFILES ON 4 FACETED SPURS IN CENTRAL 76 APENNINES

77 We focus on 4 facets formed in limestones located along 3 active faults in central Apennines
78 (Italy). Since late Pliocene-early Pleistocene, active normal faults accommodate the SW-NE
79 extension in the area (Roberts and Michetti 2004). The Velino-Magnola fault is a major
80 structure of the range (~30 km long, Fig. 1) with facets up to 300-800 m high, where we
81 sampled two sites MA1 and MA3 along the northern and central part of the fault,
82 respectively. The Roccapreturo fault is shorter (10 km), with lower facets (100-150 m), and
83 was sampled at site AR in the center of the fault. The Bazzano fault is a small (3 km long)
84 antithetic fault, with several facets reaching 100-150 m high, sampled in its southern section
85 at site BAZ (Suppl.). The surface of the 4 sampled facets displays regular slope 30-35° (Fig
86 3). The surface of the facet is characterized by an alternance of bedrock outcrop, small
87 bedrock protrusions (< 1m high), and patches of soil and screes less than a few cm thick. The
88 facets are generally bounded by entrenched non-perennial streams that flow perpendicular to
89 the fault's strike, which suggests recent incision that is contemporaneous with fault
90 development. The slopes of the colluvial wedge surface ($\alpha \sim 25\text{-}30$) and of the facets ($\gamma \sim 30\text{-}35$)
91 are similar across sites, the fault dips (β) from 40° at MA1, to 65° at BAZ (Suppl.).

92 The facets were sampled following an up-dip fault transect (Suppl.). We focused sampling on
93 the lower part of the facet, where the surface appears less rugged, and near the facet center to
94 avoid increased erosion by bounding gullies. Samples are 5-10 cm thick pieces of bedrock,
95 taken on the top of protruding (> 0.5 m) bedrock surfaces, avoiding places that could have

96 been covered by regolith. Each sample was chemically prepared for ^{36}Cl measurements
97 (Suppl.). At MA3 and ARC, the ^{36}Cl concentrations are roughly constant all along the facet
98 (Fig. 3), except at the base where they increase by about 30%. At MA1 and BAZ, facets are
99 lower and there are fewer points of measurements, but we observe a similar pattern at MA1
100 with constant values at the top, a slight decrease and an abrupt increase at the base of facet.
101 There are only 3 data points at BAZ with decreasing concentrations toward the base. The
102 ^{36}Cl concentrations along all studied facets are thus roughly **constant** suggesting that the
103 denudation rate on those features is approximately constant. This observation is consistent
104 with a facet development model that **assumes a constant denudation rate**. Moreover while it
105 has been usually assumed that erosion would vary with facet height (Tucker et al. 2020 and
106 references there in), our results suggest that, on the facet we studied, this is not the case.

107 **3-FAULT SLIP-RATE FROM ^{36}Cl DATA INVERSION**

108 To constrain the fault slip-rate we carried out a Bayesian inversion of the observed ^{36}Cl
109 concentrations where the model parameters are the individual slip-rates of the faults (SR_{MA3} ,
110 SR_{MA1} , SR_{ARC} , SR_{BAZ}), and the post-glacial period duration (T_{PG}), assumed to be the same for
111 the 4 sites (T_{exhum} is fixed a priori see suppl.). A complete description of the inversion
112 procedure using the GW-MCMC algorithm (Goodman and Weare 2010), the corresponding
113 parameters and the numerical code are provided in the Suppl. The inversion yielded mean
114 slip-rates of 3.0 ± 1.2 mm/yr for MA3, 0.2 ± 0.02 mm/yr for MA1, 0.4 ± 0.3 mm/yr for ARC,
115 and 0.06 ± 0.02 mm/yr for BAZ (Fig. 3 and 4). The mean post-glacial duration, common to all
116 sites, is 18.7 ± 2 ka.

117 The modeled ^{36}Cl concentrations **recover the average** observed values at the scale of the facet,
118 but do not account for the variability in ^{36}Cl concentrations observed in the lower part of the
119 transects (Fig. 3).

120 **4-DISCUSSION**

121 **Local controls on ^{36}Cl concentration**

122 In most cases, for the upper part, the inversion **reproduces the mean** ^{36}Cl concentration.
123 Overall, the discrepancy between observed and modeled concentrations is at most 0.5×10^5 at
124 $^{36}\text{Cl}/\text{g}$ rock except for the points at the base of each site where observed concentrations are
125 systematically higher by as much as 20% (except BAZ). The discrepancy for the upper part of
126 the profile could be attributed to the stochastic dynamics of local processes such as temporary
127 cover by a few cm of scree or abrupt removal of bedrock fragments that would lower the
128 observed amount of ^{36}Cl with respect to the predictions of our model. A scree cover of 10 cm

129 would yield a 10% decrease in ^{36}Cl concentration and could account for a large fraction of the
130 observed intra-site variability (Suppl.). On the contrary, simulations for MA3 show that a
131 scree cover of less than 5-10 cm yields an increase in [^{36}Cl]. This is due to a relatively large
132 slip-rate (3 mm/yr), and high natural chlorine content of some samples (>50 ppm) that
133 maximize ^{36}Cl production at depth 0 to 100 cm (Schimmelpfennig et al. 2009). **Another**
134 **possibility that explains such a discrepancy could be that the facet slope might be locally**
135 **steeper** than the mean value used in the model. A difference of 10° could increase ^{36}Cl
136 concentration by about 7% (Suppl.). At the base of the profile, where observed concentrations
137 are systematically higher by as much as 20% (except BAZ), the observed systematic increase
138 in ^{36}Cl concentration cannot be attributed to such short wavelength random variability in
139 surface processes. This portion is at the intersection between the bedrock scarp and the facet
140 slope, which is defined in the model by the altitude of the bedrock scarp top. There is a high
141 uncertainty in the altitude of this point, usually affected by sliding scree that could explain the
142 discrepancy. The shielding calculation might also underestimate the effect of secondary
143 neutrons produced through colluvial material or bedrock (Masarik and Wieler 2003, Balco
144 2014). The colluvial density and the dip of the colluvial slope also affect the ^{36}Cl content at
145 the base of the profile and could additionally account for this discrepancy (Suppl.).

146 **Duration of exhumation versus post-glacial exposure**

147 The value of 18.7 ± 2 ka obtained for the post-glacial duration is consistent with the timing of
148 the most important glacial retreat in the Apennines estimated at about 21 ka from lake
149 deposits records and morainic deposit (Giraudi 2017). It also corroborates the exposure ages
150 from the top of the bedrock scarp at 11-15 ka at similar sites around the Apennines (Benedetti
151 et al. 2013, Cowie et al. 2017). The amount of ^{36}Cl accumulated during the exhumation phase
152 under glacial conditions is controlled primarily by fault slip rates and accounts for 9% of the
153 total ^{36}Cl budget for MA3, 58% for MA1, 24% for ARC and 66% for BAZ. It means that at
154 MA3, 95% of the measured ^{36}Cl has been accumulated over the last 20 ka, at the other sites
155 this integration time is much longer, with durations of 185 ka, 47 ka and 210 ka at MA1, ARC
156 and BAZ, respectively. Our approach thus allows determining slip-rates averaged over time
157 scales that range from 20 to 210 ka. It is noteworthy that slower slip-rates are more tightly
158 constrained because the ^{36}Cl buildup at depth outweigh the post-glacial ^{36}Cl production.

159 **Slip-rate variability over time and relationships with facet morphology**

160 Slip-rates derived from inversion for the four studied sites are between 3 and 0.06 mm/yr
161 which is within the range of observations over the Holocene for similar faults in the
162 Apennines (Benedetti et al. 2013, Cowie et al. 2017). Sites MA3 and MA1 are less than 5 km

163 apart and located on two segments of the Magnola fault (Suppl.). ^{36}Cl exposure dating of the
164 bedrock scarp at each site yield Holocene-averaged slip rates of 1 to 1.5 mm/yr at MA3 and
165 MA1 (Schlagenhauf et al. 2011), which is comparable with the result obtained at MA3 (3 ± 1.2
166 mm/yr over 20 ka). On the other hand, the slip-rate at MA1 (0.2 ± 0.02 mm/yr over 185 ka) is
167 much lower than the one determined over the last ≈ 15 ka by Schlagenhauf et al. (2011). This
168 discrepancy may be related to the difference in time-scale, suggesting that the slip on the fault
169 has considerably accelerated over the last ≈ 15 ka. Slip-rate variability through time has
170 already been reported for the few faults worldwide where multiple time-scales records are
171 available (Perouse and Wernicke 2017, Friedrich et al. 2003). Studies on normal fault growth
172 have shown that slip-rate can be highly variable over the fault length and over time
173 (Manighetti et al. 2005). Our results confirm those observations and provide data to link
174 incremental earthquake slip events and fault growth. The Bazzano fault (site BAZ) is an
175 antithetic fault of the Paganica fault that ruptured during the 2009 L'Aquila earthquake.
176 Several studies have allowed determining the Paganica slip-rate over a few thousand years to
177 the Middle Pleistocene (Pucci et al. 2019). All converge toward a slip-rate of less than 0.4
178 mm/yr. The rate obtained for the antithetic Bazzano fault of 0.06 ± 0.02 mm/yr over the last
179 210 ka would thus account for about 15% of the Paganica synthetic fault slip, which appears
180 realistic (Boncio et al. 2010). The slip-rate at site AR of 0.4 ± 0.3 mm/yr over the last 47 ka is
181 similar to the rate previously estimated from Falcucci et al. (2015) of 0.2-0.3 mm/yr over the
182 last 1 ± 0.2 Ma.

183 The slip-rates obtained for the four sites vary with the facet height, with the highest rate at
184 MA3 where facet is 800 m-high (Schlagenhauf et al. 2011). This is in agreement with DePolo
185 and Anderson (2000) who carried out a statistical analysis on normal faults located in the
186 Basin and Range and observed a logarithmic relationship between the height of the facet and
187 the vertical slip-rate of the fault (ranging from 0.001 to 2 mm/yr). Based on numerical
188 modelling experiments, Petit et al. (2009) and Strak et al. (2011) also derived a linear
189 relationship between facet height and throw rate in agreement with our results.

190 CONCLUSIONS

191 Our study presents the first systematic CRN measurements across facets developed above
192 normal faults. We observe strikingly consistent signals with near constant ^{36}Cl concentrations
193 over the height of the studied facets, which suggests the facets are close to a morphological
194 steady state with a constant denudation during their development. Accordingly, we performed
195 inverse modeling of the concentration profiles and inferred slip rates over the last 20-200 ka,
196 the results of which are in agreement with long-term rate independently determined on some

197 of those faults over the last 1 Ma. The integration time span for ^{36}Cl accumulation over the
198 facets is longer than the postglacial history of these landscapes, suggesting that such
199 measurements could provide slip rates estimates over a time window that is usually
200 undersampled in most tectonic geomorphology studies.

201 ACKNOWLEDGMENTS

202 This work has been partly funded by the LABEX OT MED. M. Rizza and B. Ourion are
203 greatly acknowledged for their help and support in the field.

204 FIGURES CAPTIONS

205 Fig. 1 : A) Tectonic map of the Lazio-Abruzzo fault system (Schlagenhauf et al. 2011,
206 Benedetti et al. 2013) with the faults (red line) bounding the sampled facets (yellow arrows)
207 and site names (sites names were kept as in Schlagenhauf et al. 2010). B) Photography of the
208 F-MA1 facet with location of samples and Holocene bedrock fault scarp at the base of the
209 facets.

210 Fig. 2 : A-Modelled topographic profile of normal escarpment following Tucker et. al (2011)
211 model resulting from exhumation of the footwall, with slope of the colluvial wedge surface α ,
212 dipping angle of fault-plane β , and γ slope of facet surface.

213 Fig. 3 : Measured (black dot) and modeled ^{36}Cl concentrations obtained from Bayesian
214 inversion (grey pdf) of samples collected on the 4 facets (MA3, MA1, AR, BAZ) in Central
215 Italy, as a function of sample altitude. Reduced chi-squared values are MA3=6.4; MA1=8.2;
216 AR=5.2; BAZ=19.6.

217 Fig. 4 : Results from Bayesian inversion of ^{36}Cl data acquired on facet. Probability densities
218 are plotted as function of slip-rate and post-glacial period duration (T_{pg}), with contour lines
219 representing 10, 30, 50, 70, 90 % highest density interval. Pdf of posterior distribution is also
220 shown for each SR and for T_{pg} .

221 REFERENCES CITED

222 Allen, J. R. M. et al. Rapid environmental changes in southern Europe during the last glacial
223 period. *Nature* 400, 740–743 (1999).

224 Armijo, R., Tapponnier, P., Mercier, J. L., & Han, T. L. (1986). Quaternary extension in
225 southern Tibet: Field observations and tectonic implications. *Journal of Geophysical*
226 *Research: Solid Earth*, 91(B14), 13803-13872.

227

228 Armijo, R., Lyon-Caen, H., & Papanastassiou, D. (1992). East-west extension and Holocene
229 normal-fault scarps in the Hellenic arc. *Geology*, 20(6), 491-494.
230

231 Balco, G. (2014). Simple computer code for estimating cosmic-ray shielding by oddly shaped
232 objects. *Quaternary Geochronology*, 22, 175-182.
233

234 Benedetti, L., Manighetti, I., Gaudemer, Y., Finkel, R., Malavieille, J., Pou, K., ... &
235 Keddadouche, K. (2013). Earthquake synchrony and clustering on Fucino faults (Central
236 Italy) as revealed from in situ ³⁶Cl exposure dating. *Journal of Geophysical Research: Solid*
237 *Earth*, 118(9), 4948-4974.
238

239 Boncio, P., Pizzi, A., Brozzetti, F., Pomposo, G., Lavecchia, G., Di Naccio, D., & Ferrarini,
240 F. (2010). Coseismic ground deformation of the 6 April 2009 L'Aquila earthquake (central
241 Italy, Mw6. 3). *Geophysical Research Letters*, 37(6).
242

243 Burbank, D. W., & Anderson, R. S. (2011). *Tectonic geomorphology*. John Wiley & Sons.
244

245 Cowie, P. A., Phillips, R. J., Roberts, G. P., McCaffrey, K., Zijerveld, L. J. J., Gregory, L. C.,
246 ... & Freeman, S. P. H. T. (2017). Orogen-scale uplift in the central Italian Apennines drives
247 episodic behaviour of earthquake faults. *Scientific reports*, 7, 44858.
248

249 DePolo, C. M., & Anderson, J. G. (2000). Estimating the slip rates of normal faults in the
250 Great Basin, USA. *Basin Research*, 12(3-4), 227-240.
251

252 Friedrich, A. M., Wernicke, B. P., Niemi, N. A., Bennett, R. A., & Davis, J. L. (2003).
253 Comparison of geodetic and geologic data from the Wasatch region, Utah, and implications
254 for the spectral character of Earth deformation at periods of 10 to 10 million years. *Journal of*
255 *Geophysical Research: Solid Earth*, 108(B4).
256

257 Giraudi, C., & Giaccio, B. (2017). Middle Pleistocene glaciations in the Apennines, Italy: new
258 chronological data and preservation of the glacial record. *Geological Society, London, Special*
259 *Publications*, 433(1), 161-178.
260

261 Gold, R. D., Cowgill, E., Arrowsmith, J. R., & Friedrich, A. M. (2017). Pulsed strain release
262 on the Altyn Tagh fault, northwest China. *Earth and Planetary Science Letters*, 459, 291-300.
263

264 Goodman, J., & Weare, J. (2010). Ensemble samplers with affine
265 invariance. *Communications in applied mathematics and computational science*, 5(1), 65-80.
266

267 Mitchell, S. G., Matmon, A., Bierman, P. R., Enzel, Y., Caffee, M., & Rizzo, D. (2001).
268 Displacement history of a limestone normal fault scarp, northern Israel, from cosmogenic
269 ^{36}Cl . *Journal of Geophysical Research: Solid Earth*, 106(B3), 4247-4264.
270

271 Masarik, J., & Wieler, R. (2003). Production rates of cosmogenic nuclides in boulders. *Earth
272 and Planetary Science Letters*, 216(1-2), 201-208.
273

274 Manighetti, I., Campillo, M., Sammis, C., Mai, P. M., & King, G. (2005). Evidence for self-
275 similar, triangular slip distributions on earthquakes: Implications for earthquake and fault
276 mechanics. *Journal of Geophysical Research: Solid Earth*, 110(B5).
277

278 Petit, C., Gunnell, Y., Gonga-Saholiariliva, N., Meyer, B., & Séguinot, J. (2009b). Faceted
279 spurs at normal fault scarps: Insights from numerical modeling. *Journal of Geophysical
280 Research: Solid Earth*, 114(B5).
281

282 Pérouse, E., & Wernicke, B. P. (2017). Spatiotemporal evolution of fault slip rates in
283 deforming continents: The case of the Great Basin region, northern Basin and Range
284 province. *Geosphere*, 13(1), 112-135.
285

286 Pucci, S., Villani, F., Civico, R., Di Naccio, D., Porreca, M., Benedetti, L., ... & Pantosti, D.
287 (2019). Complexity of the 2009 L'Aquila earthquake causative fault system (Abruzzi
288 Apennines, Italy) and effects on the Middle Aterno Quaternary basin
289 arrangement. *Quaternary Science Reviews*, 213, 30-66.
290

291 Roberts, G. P., and A. M. Michetti (2004), Spatial and temporal variations in growth rates
292 along active normal fault systems: an example from The Lazio–Abruzzo Apennines, central
293 Italy, *J. Struct. Geol.*, 26(2), 339–376, doi:10.1016/S0191-8141(03)00103-2.
294

295 Roberts, G. P., Raithatha, B., Sileo, G., Pizzi, A., Pucci, S., Walker, J. F., ... & Guerrieri, L.
296 (2010). Shallow subsurface structure of the 2009 April 6 M w 6.3 L'Aquila earthquake
297 surface rupture at Paganica, investigated with ground-penetrating radar. *Geophysical Journal*
298 *International*, 183(2), 774-790.

299

300 Ryerson, F.J., Tapponnier, P., Finkel, R.C., Mériaux, A.-S., Van der Woerd, J., Lasserre, C.,
301 Chevalier, M.-L., Xu, X., Li, H., and King, G.C.P., 2006, Applications of morphochronology
302 to the active tectonics of Tibet, in Siame, L.L., Bourlès, D.L., and Brown, E.T., eds.,
303 Application of cosmogenic nuclides to the study of Earth surface processes: The practice and
304 the potential: Geological Society of America Special Paper 415, p. 61–86, doi:
305 10.1130/2006.2415(05).

306

307 Schimmelpfennig, I., Benedetti, L., Finkel, R., Pik, R., Blard, P. H., Bourles, D., ... &
308 Williams, A. (2009). Sources of in-situ ³⁶Cl in basaltic rocks. Implications for calibration of
309 production rates. *Quaternary Geochronology*, 4(6), 441-461.

310

311 Schlagenhauf, A., Gaudemer, Y., Benedetti, L., Manighetti, I., Palumbo, L.,
312 Schimmelpfennig, I., ... & Pou, K. (2010). Using in situ Chlorine-36 cosmonuclide to recover
313 past earthquake histories on limestone normal fault scarps: a reappraisal of methodology and
314 interpretations. *Geophysical Journal International*, 182(1), 36-72.

315

316 Schlagenhauf, A., Manighetti, I., Benedetti, L., Gaudemer, Y., Finkel, R., Malavieille, J., &
317 Pou, K. (2011). Earthquake supercycles in Central Italy, inferred from ³⁶Cl exposure
318 dating. *Earth and Planetary Science Letters*, 307(3-4), 487-500.

319

320 Strak, V., Dominguez, S., Petit, C., Meyer, B., & Loget, N. (2011). Interaction between
321 normal fault slip and erosion on relief evolution: Insights from experimental
322 modelling. *Tectonophysics*, 513(1-4), 1-19.

323

324 Tucker, G. E., McCoy, S. W., Whittaker, A. C., Roberts, G. P., Lancaster, S. T., & Phillips, R.
325 (2011). Geomorphic significance of postglacial bedrock scarps on normal-fault
326 footwalls. *Journal of Geophysical Research: Earth Surface*, 116(F1).

327

328 Tucker, G. E., Hobbey, D. E., McCoy, S. W., & Struble, W. T. Modeling the Shape and
329 Evolution of Normal-Fault Facets. *Journal of Geophysical Research: Earth Surface*,
330 e2019JF005305.

331

332 Wallace, R. E. (1978). Geometry and rates of change of fault-generated range fronts, north-
333 central Nevada. *J. Res. US Geol. Surv*, 6(5), 637-650.

334